hyperactivated *NP394-neurons* showed promoted light avoidance, we propose that *NP394-neuron* activity is positively correlated with larval light-avoidance ability. Two possible scenarios could be operating in this situation. First, the activity of *NP394-neurons* itself controls the larval phototaxis by an unknown mechanism. Second, the *NP394-neurons* activate the pathway that mediates avoidance of light whereas other unidentified neurons activate the pathway that underlies avoidance of darkness, as was shown for the mechanisms underlying odor-taxis in adult *Drosophila* (*25*).

References and Notes

1. J. N. Crawley, *What's Wrong With My Mouse? Behavioral Phenotyping of Transgenic and Knockout Mice* (Wiley, New York, 2000).
2. M. Manning, T. A. Markow, *Behav. Genet.* **11**, 557 (1981).
3. J. Grossfield, *Proc. Natl. Acad. Sci. U.S.A.* **68**, 2669 (1971).
4. Y. Ben-Shahar, H. T. Leung, W. L. Pak, M. B. Sokolowski, G. E. Robinson, *J. Exp. Biol.* **206**, 2507 (2003).
5. F. P. Sawin, L. R. Harris, A. R. Campos, M. B. Sokolowski, *J. Insect Behav.* **7**, 553 (1994).
6. E. O. Mazzoni, C. Desplan, J. Blau, *Neuron* **45**, 293 (2005).
7. E. P. Sawin-McCormack, M. B. Sokolowski, A. R. Campos, *J. Neurogenet.* **10**, 119 (1995).
8. C. Helfrich-Förster *et al.*, *J. Neurosci.* **22**, 9255 (2002).
9. S. G. Sprecher, C. Desplan, *Nature* **454**, 533 (2008).
10. S. Malpel, A. Klarsfeld, F. Rouyer, *Development* **129**, 1443 (2002).
11. J. Hassan, B. Iyengar, N. Scantlebury, V. Rodriguez Moncalvo, A. R. Campos, *J. Comp. Neurol.* **481**, 266 (2005).
12. M. Busto, B. Iyengar, A. R. Campos, *J. Neurosci.* **19**, 3337 (1999).
13. S. T. Sweeney, K. Broadie, J. Keane, H. Niemann, C. J. O'Kane, *Neuron* **14**, 341 (1995).
14. M. N. Nitabach, J. Blau, T. C. Holmes, *Cell* **109**, 485 (2002).
15. A. M. van der Bliek, E. M. Meyerowitz, *Nature* **351**, 411 (1991).
16. M. N. Nitabach *et al.*, *J. Neurosci.* **26**, 479 (2006).
17. C. H. Yang *et al.*, *Neuron* **61**, 519 (2009).
18. H. Dircksen *et al.*, *Cell Tissue Res.* **250**, 377 (1987).
19. W. Li *et al.*, *Cell Tissue Res.* **336**, 509 (2009).
20. J. Wang *et al.*, *Neuron* **43**, 663 (2004).
21. E. H. Feinberg *et al.*, *Neuron* **57**, 353 (2008).
22. M. D. Gordon, K. Scott, *Neuron* **61**, 373 (2009).
23. Y. Shang, L. C. Griffith, M. Rosbash, *Proc. Natl. Acad. Sci. U.S.A.* **105**, 19587 (2008).
24. L. Tian *et al.*, *Nat. Methods* **6**, 875 (2009).
25. J. L. Semmelhack, J. W. Wang, *Nature* **459**, 218 (2009).

26. We thank K. Rao for antibody to Pdf; J. Blau, K. Scott, M. Rosbach, T. Lee, C. Feng, Y. Zhong, W. Yi, Y. Jan, and R. Jiao for fly stocks and constructs; and C. Wang and X. Hao for facility setup. We thank the DGRC (Kyoto) and the Bloomington fly stock center for the fly stocks, and Developmental Studies Hybridoma Bank for antibodies. We also thank H. Gong for technical assistance, and J. Fleming and R. Wolf for valuable comments. This work was supported by the National Natural Sciences Foundation of China [grant 30770682 (Z.G.) and grants 30621004 and 30625022 (L.L.)], the '973 Program' [grants 2005CB522804 and 2009CB918702 (L.L.)], and the Knowledge Innovation Program of the Chinese Academy of Sciences [grant KSCX2-YW-R-247 (L.L.)].

Supporting Online Material

www.sciencemag.org/cgi/content/full/330/6003/499/DC1
Materials and Methods
Figs. S1 to S13
Table S1
References
Movies S1 to S3

3 August 2010; accepted 8 September 2010
10.1126/science.1195993

Fast Vesicle Fusion in Living Cells Requires at Least Three SNARE Complexes

Ralf Mohrmann,[1,2]* Heidi de Wit,[3] Matthijs Verhage,[3] Erwin Neher,[1] Jakob B. Sørensen[1,4,5]*

Exocytosis requires formation of SNARE [soluble *N*-ethylmaleimide–sensitive factor attachment protein (SNAP) receptor] complexes between vesicle and target membranes. Recent assessments in reduced model systems have produced divergent estimates of the number of SNARE complexes needed for fusion. Here, we used a titration approach to answer this question in intact, cultured chromaffin cells. Simultaneous expression of wild-type SNAP-25 and a mutant unable to support exocytosis progressively altered fusion kinetics and fusion-pore opening, indicating that both proteins assemble into heteromeric fusion complexes. Expressing different wild-type:mutant ratios revealed a third-power relation for fast (synchronous) fusion and a near-linear relation for overall release. Thus, fast fusion typically observed in synapses and neurosecretory cells requires at least three functional SNARE complexes, whereas slower release might occur with fewer complexes. Heterogeneity in SNARE-complex number may explain heterogeneity in vesicular release probability.

The SNARE [soluble *N*-ethylmaleimide–sensitive factor attachment protein (SNAP) receptor] complex formed between two fusing membranes is at the heart of the molecular machinery that mediates exocytosis (*1*). It is a coiled bundle of four parallel α helices provided by three SNARE proteins: SNAP-25 (synaptosome-associated protein of 25 kD), synaptobrevin-2, and syntaxin-1 (*2*). SNARE-complex formation proceeds from the N- to the C-terminal end in a discontinuous process that involves partially assembled intermediates. Assembly of the most C-terminal three to four interaction layers coincides with membrane merger (*3*). Though it has been unclear whether assembly of one SNARE complex generates sufficient energy to initiate vesicle fusion (*4*–*7*), it was recently reported that liposomes can fuse with the help of a single SNARE complex, albeit with low speed (*8*). Other studies have concluded that 5 to 11 SNARE complexes might be involved in faster modes of fusion (*9*–*13*).

To study the dependence of fast vesicle fusion on higher-order SNARE complexes in intact cells, we used an exceptionally inhibitory SNAP-25 mutation in a titration assay that allowed us to relate exocytosis to the relative expression levels of mutant and wild-type (WT) protein in a given cell. Our mutant harbored two alanine substitutions [$Met^{71} \rightarrow Ala^{71}$ (M71A) and $Ile^{92} \rightarrow Ala^{92}$ (I192A)] in the interaction layer +5, facing the inside of the complex (*2*). If incorporated in the SNAP-25A isoform, this mutation completely fails to reconstitute exocytosis in *Snap-25*$^{-/-}$ adrenal chromaffin cells (*14*). Here, we introduced the mutation into SNAP-25B, because this isoform supports two to three times more fast-phase secretion (*15*). SNAP-25B WT (SN25B) or mutant protein (denoted SN25BL5**) were N-terminally fused to enhanced green fluorescent protein (EGFP) or mCherry (mCh), allowing for the quantitative analysis of expression levels and protein localization.

Using the Semliki Forest virus (SFV) expression system, we characterized mCh-tagged SN25BL5** and mCh-SN25B expressed separately in SNAP-25–deficient chromaffin cells (*16*). Both proteins were localized to the plasma membrane and expressed to similar levels (Fig. 1, E and F). Secretion was assayed by membrane capacitance measurements and amperometry after flash photorelease of caged calcium. Expression of mCh-SN25BL5** suppressed secretion (total capacitance change: 12 ± 3 fF after 5 s; $n = 28$ cells) (Fig. 1, A to E) compared with mCh-SN25B–infected cells (510 ± 54 fF; $n = 36$; $P < 0.0001$) and even SNAP-25–deficient cells (39 ± 5 fF; $n = 35$; $P < 0.0001$; Student's t test). This made SN25BL5** an attractive inhibitor for a titration experiment. Several lines of evidence indicate that inhibition probably arises from interference with a very late step of exocytosis associated with the C-terminal assembly of the SNARE complex: (i) SN25L5** forms stable SNARE complexes

[1]Department of Membrane Biophysics, Max-Planck Institute for Biophysical Chemistry, Göttingen, Germany. [2]Department of Physiology, University of Saarland, Homburg, Germany. [3]Center for Neurogenomics and Cognitive Research, Department of Functional Genomics, Vrije Universiteit (VU) Amsterdam and VU Medical Center, Amsterdam, Netherlands. [4]Department of Neuroscience and Pharmacology, Faculty of Health Sciences, University of Copenhagen, Copenhagen, Denmark. [5]Lundbeck Foundation Center for Biomembranes in Nanomedicine, University of Copenhagen, Copenhagen, Denmark.

*To whom correspondence should be addressed. E-mail: Ralf.Mohrmann@uks.eu (R.M.); jakobbs@sund.ku.dk (J.B.S.)

in vitro, exhibiting assembly kinetics indistinguishable from WT protein (*14*). However, mutant SNARE complexes exhibit a strongly destabilized C-terminal end (*14*). (ii) SNAP-25 is required for vesicle docking (*17*) before participating in downstream steps of exocytosis. Expression of SN25BL5** completely restored docking in *Snap-25*$^{-/-}$ cells (Fig. 1, G to I, and fig. S1), excluding an involvement of layer +5 in these early steps of exocytosis. (iii) The phenotypes caused by single point mutations in layer +5 of SN25B (M71A or I192A) indicate that assembly of this layer is important for fusion triggering. Expression of either mutant in *Snap-25*$^{-/-}$ cells slowed down fusion kinetics (fig. S2, A and B), similar to other mutations compromising the C-terminal end of the SNARE complex (*14*, *18*). In contrast, unchanged sustained-release rates (fig. S2Ab and S2Bb) and normal recovery between stimulations (fig. S2Ae and S2Be) suggest normal vesicle priming.

To obtain cells with varying ratios of mCh-SN25BL5** and EGFP-SN25B, we generated viruses harboring bicistronic expression units containing different "internal ribosome entry site" (IRES)–sequences (fig. S3) (*16*). After calibration with an EGFP-mCh fusion protein (fig. S3B), relative expression levels of the two fusion proteins were assessed by quantifying mCh and EGFP fluorescence. All viruses displayed substantial variations of expression ratios in individual cells, which were exploited to cover a wider range of expression ratios. The two fusion proteins colocalized closely (fig. S4), both on the plasma membrane and on certain intracellular structures (*19*).

In control recordings, EGFP-SN25B–expressing cells exhibited an average total capacitance increase of 483 ± 25 fF (n = 125). Progressively increasing fractional mCh-SN25BL5** expression

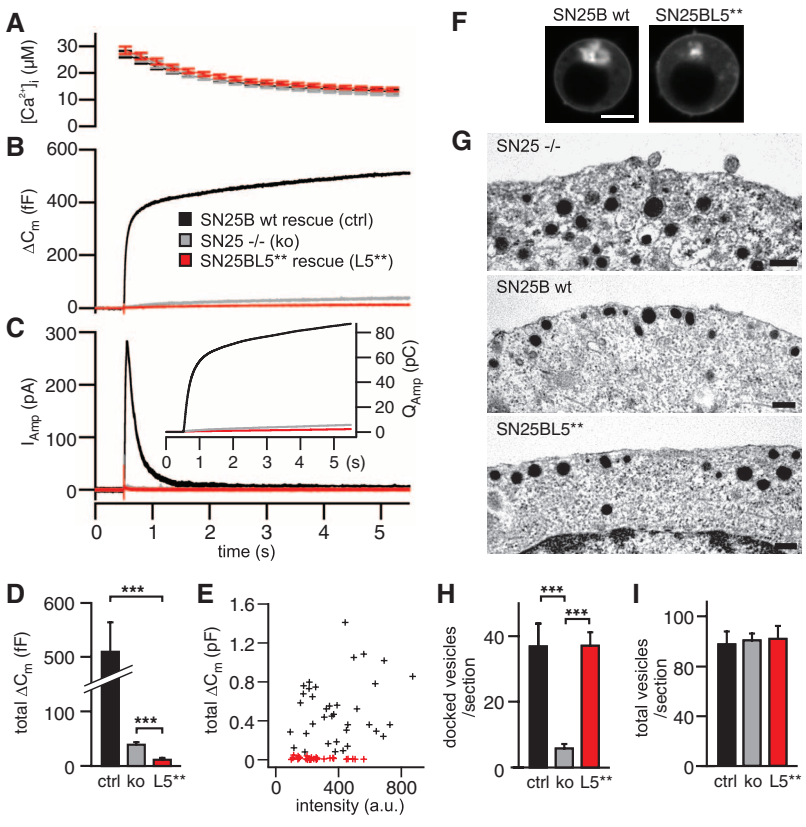

Fig. 1. A SNAP-25B mutant causes complete arrest of neurotransmitter release. (**A** to **C**) Averaged data for calcium uncaging experiments in *Snap-25*–deficient chromaffin cells (ko, knockout) (gray), knockout cells expressing mCh-SN25B wild type (ctrl) (black), or mCh-SN25B M71A, I192A (SN25BL5**; L5**) (red). (A) Intracellular calcium concentrations (mean ± SEM) after ultraviolet flash applied at 0.5 s. $[Ca^{2+}]_i$, intracellular concentration of Ca^{2+}. (B) Induced membrane capacitance change (ΔC_m). (C) Amperometric current (I_{Amp}). (Inset) Cumulative amperometric charge (Q_{Amp}). (**D**) Total capacitance change (mean ± SEM) reached after 5 s was significantly (***$P < 0.0001$, Student's t test) decreased by expression of SN25BL5**. (**E**) Plot of total capacitance change versus cellular fluorescence intensity. a.u., arbitrary units. (**F**) Confocal microphotographs of chromaffin cells expressing mCh-SN25B or mCh-SN25BL5**. Scale bar, 5 μm. (**G**) Sample electron micrographs of *Snap-25* knockout cell and knockout cell expressing WT SN25B or SN25BL5**. Scale bars, 200 nm. (**H**) Number of docked vesicles and (**I**) total number of vesicles (mean ± SEM) in *Snap-25* knockout cells and after rescue with SN25BL5** and WT protein (***$P < 0.001$).

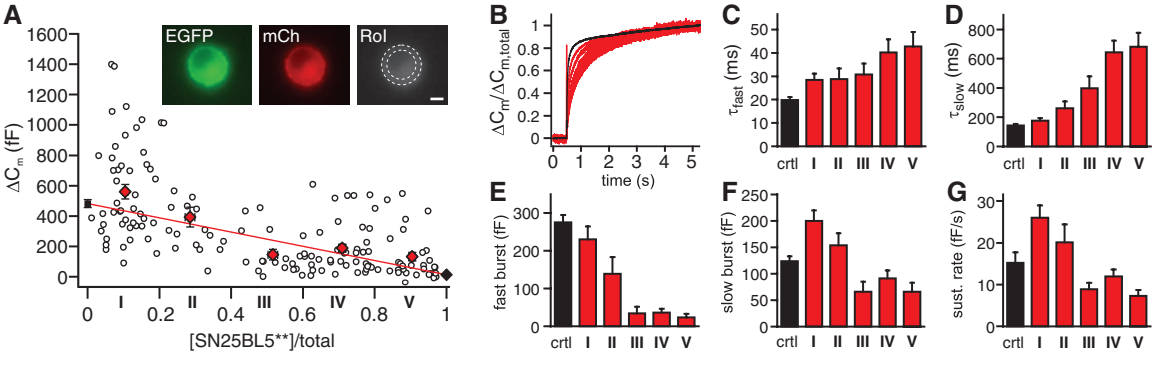

Fig. 2. Coexpression of SN25L5** with WT SNAP-25 is accompanied by a pronounced slowdown of release. (**A**) Plot of the overall capacitance change (5 s after flash) versus the fraction of mutant SNAP-25 expressed. Open circles represent single recordings; red diamonds denote mean data for five (I to V) binned groups; black symbols represent the capacitance change in cells expressing only EGFP-SN25B (0%) or mCh-SN25BL5** (100%). The red line indicates a strict linear relation between a fraction of SN25BL5** and inhibition, assuming no cooperativity. Error bars represent SEM. (Inset) Microphotographs of a chromaffin cell expressing both SNAP-25 variants. Fluorescence intensity was measured in a region of interest (RoI) enclosing the plasma membrane. Scale bar, 5 μm. (**B** to **D**) Kinetic analysis of capacitance changes. (B) Capacitance traces were averaged in each binned group (I to V, red; EGFP-SN25B, black) and normalized to their amplitude at 5 s. (C) Fast and (D) slow bursts show gradually increasing time constants (τ_{fast} and τ_{slow}, respectively) during titration with SN25BL5**. (**E**) The amplitude of the fast burst steadily decreases during the titration, whereas (**F**) slow-burst amplitude and (**G**) the rate of sustained release pass through a transient maximum to eventually diminish. All values are given as mean ± SEM.

had a mild inhibitory effect on overall exocytosis (Fig. 2A). The inhibition profile was well described by a linear dependency on the fraction of mCh-SN25BL5**. Kinetic analysis revealed a progressive slowdown of release kinetics (Fig. 2B), owing to a gradual increase of fast- and slow-burst time constants (Fig. 2, C and D) combined with decreased amplitude of the fast component (Fig. 2E). For cells expressing low levels of mCh-SN25BL5** (0 to 20%, group I), the decrease in fast-release amplitude was partly compensated for by an increase in slow-burst amplitude (Fig. 2F) and in the rate of sustained secretion (Fig. 2G). Overall, vesicles fuse at lower rates in the presence of SN25BL5**, implying that the vesicular release probability is decreased. Because exocytosis cannot be mediated by fusion complexes solely containing SN25BL5**, this finding indicates the formation of mixed fusion complexes containing both EGFP-SN25B and mCh-SN25BL5**.

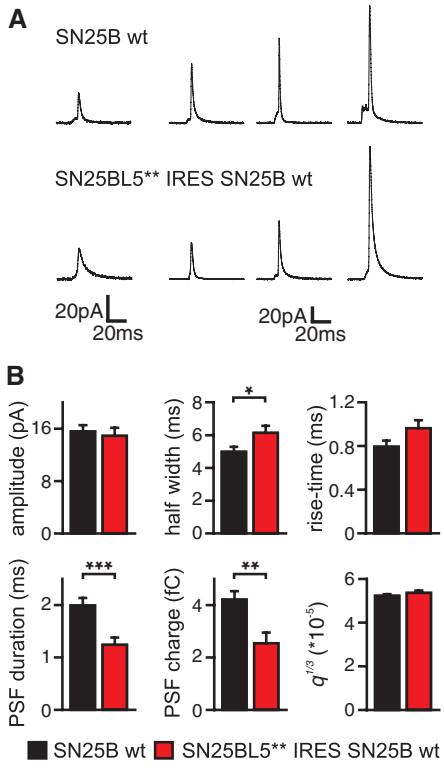

Fig. 3. Altered amperometric spikes in the presence of SN25BL5** indicate the existence of heteromeric fusion complexes. (**A**) Examples showing amperometric spikes in control cells (*Snap-25*$^{-/-}$ expressing EGFP-SN25B) and cells coexpressing WT and mutant SNAP-25B (mCh-SN25BL5**-IRES-EGFP-SN25B). (**B**) Quantitative analysis. The means of cell medians for each parameter ± SEM are shown (*q*, total charge). The half width was slightly prolonged in the presence of SN25BL5** ($P < 0.05$). The pre-spike foot duration and charge were reduced, indicating altered fusion-pore opening (**$P < 0.01$ and ***$P < 0.001$; Student's *t* test).

Formation of mixed fusion complexes was also supported by experiments examining single-vesicle fusion events (Fig. 3). In these experiments, *Snap-25*$^{-/-}$ cells were infected with a SFV expressing ~80% mCh-SN25BL5** and ~20% EGFP-SN25B (fig. S3D). In the presence of mCh-SN25BL5**, amperometric spikes exhibited a slightly delayed overall waveform and a decreased duration of pre-spike feet (PSF). Because mCh-SN25BL5** cannot support exocytosis on its own, these data indicate single-vesicle fusion using mixed complexes. A similar reduction in PSF duration has been described upon mutating the C-terminal layers of synaptobrevin-2 (*18*).

The above findings suggested that multiple SNARE complexes might surround the nascent fusion pore (*12*). Thus, we asked how many SNARE complexes are needed for fast vesicle fusion. Assuming that the incorporation of one copy of SN25BL5** is sufficient to decrease the vesicular release rate, vesicle fusion with normal fast kinetics should be mediated by complexes containing exclusively WT SN25B. The number of such vesicles depends on the fractional availability of WT SN25B raised to a power of *n*, where *n* is the number of SN25B molecules in the fusion complex (*20*). To determine the amount of fusion with unperturbed kinetics, we repeated the kinetic analysis, but this time we fixed the fast time constant τ_{fast} to the control value (EGFP-SN25B, τ_{fast} = 19.8 ms), such that the amplitude reports unperturbed secretion. The number of fast-fusing vesicles diminished much faster than overall secretion with an increasing proportion of mCh-SN25BL5** (Fig. 4A, compare with Fig. 2A). Fitting of a simple binomial model (*21*) to the entire curve identified $n = 2.8$. Alternatively, we fitted a straight line to the left part of the curve, following logarithmic transform of the burst am-

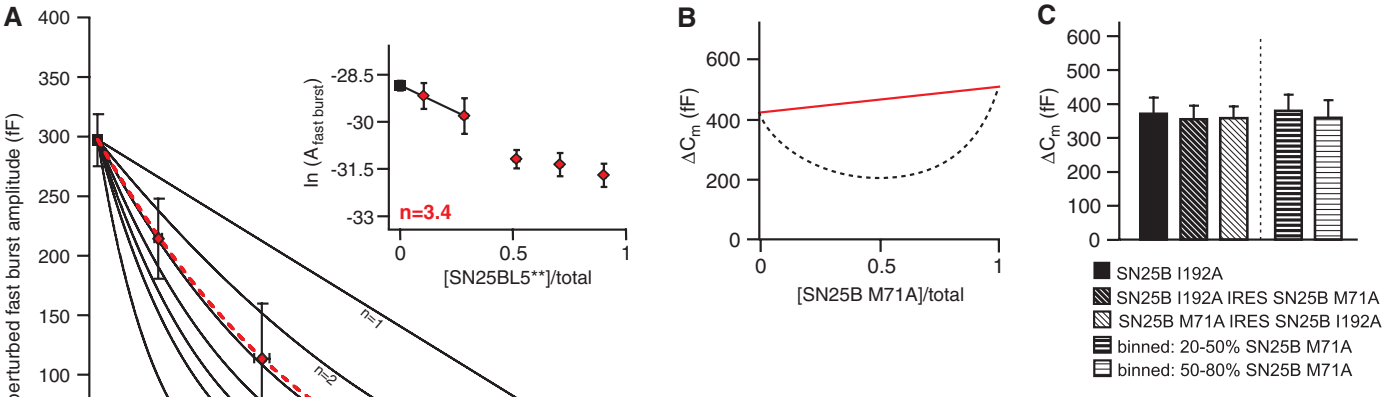

Fig. 4. Fast-fusing vesicles display higher-order dependence on the availability of SNAP-25. (**A**) Plot of unperturbed fast-burst amplitude versus SN25BL5** fraction (mean ± SEM). Fit of a binomial model (*20*) yielded $n = 2.8$ or 3.4 after the logarithmic transform, respectively (inset), interpreted as the number of SNARE complexes driving fast vesicles. The black square denotes fast-burst amplitude ($A_{fast\ burst}$), as derived for WT SN25B-expressing control cells. (**B**) If SNAP-25 cross-links SNARE complexes, coexpression of both single mutations should cause maximal inhibition at a 1:1 ratio of the two mutants (dashed line); otherwise, secretion should follow a linear interpolation line (red solid line). (**C**) Secretion was not inhibited in cells coexpressing SN25BM71A and SN25BI192A compared with reference recordings (SN25B I19A). Error bars indicate mean ± SEM. Examining data in the 20-to-50% or 50-to-80% expression bins also did not reveal any inhibition.

plitude (*21*), which yielded $n = 3.4$ (inset, Fig. 4A). Our model assumes that the affinity of SN25BL5** to the rest of the fusion apparatus is unchanged, which appears likely from previous data (*14*). Three is a lower estimate of the number of SNARE complexes in a fusion complex driving fast fusion, because incorporation of more than one mutant might be required to detectably change fusion kinetics.

SNAP-25 harbors two SNARE domains and could possibly contribute these to different SNARE complexes, thereby cross-linking them (*21*, *22*). This would separate the two single mutations and mask a dominant-negative effect of SN25BL5** in the presence of WT protein (fig. S5A), which could provide an alternative explanation for the shallow dependence of overall secretion on SN25BL5** fraction (Fig. 2A). We tested such "domain-swapping" by coexpression of the two single-layer +5 mutants (M71A and I192A). At similar expression levels, the two single alanines should recreate the catastrophic double-layer +5 mutation in half of the complexes (fig. S5B), which should result in a 50% drop in secretion (Fig. 4B, according to Fig. 2A). Using two bicistronic SFVs that express both mutants at the proportions [mCh-SN25M71A]/total of 15 ± 1% or 65 ± 3%, we observed no inhibitory effect on secretion (Fig. 4C). In addition, examining data in 20-to-50% or 50-to-80% expression bins did not identify any block of release (Fig. 4C). Thus, domain-swapping cannot explain the mild inhibition by SN25BL5**, nor can it represent a prominent event during exocytosis, consistent with the finding that separated SNAP-25 SNARE domains support in vitro vesicle fusion (*23*) and secretion (*24*).

Using a titration approach in intact cells, we report here that the apparent cooperativity for fast-phase secretion is higher (~3) than that for overall exocytosis (~1). We conclude that SNARE complexes form higher-order functional units, and at least three SNARE complexes are required for the fast phase of exocytosis (fig. S5, C and D). Our findings agree with data from infusion of synaptobrevin fragments into PC12 cells (*11*). The linear titration profile of overall secretion might be explained if stoichiometry of fusion complexes is not fixed. Vesicles resident at the plasma membrane have time to form several SNARE complexes in the absence of stimulation, achieving faster speeds of fusion when triggered by calcium. However, vesicles arriving during conditions of sustained high calcium concentrations might fuse using fewer [or possibly only a single (*8*)] SNARE complexes. The dramatic shift in release rate upon coexpression of SN25BL5** suggests that the number of functional (that is, completely zippering) SNARE complexes is a determinant of fusion probability. Indeed, variable fusion stoichiometry might underlie heterogeneity in vesicular release probabilities between synapses (*25*) or release phases (*26*) and could represent an important regulated parameter in neurotransmitter-releasing cells.

References and Notes

1. R. Jahn, R. H. Scheller, *Nat. Rev. Mol. Cell Biol.* **7**, 631 (2006).
2. R. B. Sutton, D. Fasshauer, R. Jahn, A. T. Brunger, *Nature* **395**, 347 (1998).
3. J. B. Sørensen, *Annu. Rev. Cell Dev. Biol.* **25**, 513 (2009).
4. F. Li *et al.*, *Nat. Struct. Mol. Biol.* **14**, 890 (2007).
5. K. Wiederhold, D. Fasshauer, *J. Biol. Chem.* **284**, 13143 (2009).
6. A. Yersin *et al.*, *Proc. Natl. Acad. Sci. U.S.A.* **100**, 8736 (2003).
7. W. Liu, V. Montana, V. Parpura, U. Mohideen, *Biophys. J.* **95**, 419 (2008).
8. G. van den Bogaart *et al.*, *Nat. Struct. Mol. Biol.* **17**, 358 (2010).
9. M. K. Domanska, V. Kiessling, A. Stein, D. Fasshauer, L. K. Tamm, *J. Biol. Chem.* **284**, 32158 (2009).
10. E. Karatekin *et al.*, *Proc. Natl. Acad. Sci. U.S.A.* **107**, 3517 (2010).
11. Y. Hua, R. H. Scheller, *Proc. Natl. Acad. Sci. U.S.A.* **98**, 8065 (2001).
12. C. Montecucco, G. Schiavo, S. Pantano, *Trends Biochem. Sci.* **30**, 367 (2005).
13. X. Han, C.-T. Wang, J. Bai, E. R. Chapman, M. B. Jackson, *Science* **304**, 289 (2004); published online 11 March 2004 (10.1126/science.1095801).
14. J. B. Sørensen *et al.*, *EMBO J.* **25**, 955 (2006).
15. J. B. Sørensen *et al.*, *Cell* **114**, 75 (2003).
16. Materials and methods are available as supporting material on *Science* Online.
17. H. de Wit *et al.*, *Cell* **138**, 935 (2009).
18. A. M. Walter, K. Wiederhold, D. Bruns, D. Fasshauer, J. B. Sørensen, *J. Cell Biol.* **188**, 401 (2010).
19. Y. Aikawa, K. L. Lynch, K. L. Boswell, T. F. Martin, *Mol. Biol. Cell* **17**, 2113 (2006).
20. A derivation of the rosette model of SNARE complexes is available as supporting material on *Science* Online.
21. D. H. Kweon *et al.*, *Biochemistry* **41**, 5449 (2002).
22. H. Tokumaru *et al.*, *Cell* **104**, 421 (2001).
23. F. Parlati *et al.*, *Proc. Natl. Acad. Sci. U.S.A.* **96**, 12565 (1999).
24. Y. A. Chen, S. J. Scales, S. M. Patel, Y. C. Doung, R. H. Scheller, *Cell* **97**, 165 (1999).
25. C. Rosenmund, J. D. Clements, G. L. Westbrook, *Science* **262**, 754 (1993).
26. Y. Goda, C. F. Stevens, *Proc. Natl. Acad. Sci. U.S.A.* **91**, 12942 (1994).

27. We thank I. Herfort and D. Reuter for expert technical assistance and S. Young for help with viral expression systems. This work was supported by the Lundbeck Foundation (Junior Group Leader Fellowship, J.B.S.), the Lundbeck Foundation Center for Biomembranes in Nanomedicine (J.B.S.), the Danish Medical Research Council (J.B.S.), the Netherlands Organization for Scientific Research (Pionier/VICI900-01-001 and ZonMW 903-42-095 to M.V. and VENI 916-36-043 to H.d.W.), the NeuroBsik Mouse Phenomics Consortium (BSIK03053), and the European Union Seventh Framework Programme under grant agreement no. HEALTH-F2-2009-242167 ("SynSys" project to both J.B.S. and M.V.).

Supporting Online Material

www.sciencemag.org/cgi/content/full/science.1193134/DC1
Materials and Methods
SOM Text
Figs. S1 to S5
References

2 June 2010; accepted 27 August 2010
Published online 16 September 2010;
10.1126/science.1193134
Include this information when citing this paper.

Mechanisms of Proton Conduction and Gating in Influenza M2 Proton Channels from Solid-State NMR

Fanghao Hu, Wenbin Luo, Mei Hong*

The M2 protein of influenza viruses forms an acid-activated tetrameric proton channel. We used solid-state nuclear magnetic resonance spectroscopy to determine the structure and functional dynamics of the pH-sensing and proton-selective histidine-37 in M2 bound to a cholesterol-containing virus-envelope-mimetic membrane so as to better understand the proton conduction mechanism. In the high-pH closed state, the four histidines form an edge-face π-stacked structure, preventing the formation of a hydrogen-bonded water chain to conduct protons. In the low-pH conducting state, the imidazoliums hydrogen-bond extensively with water and undergo microsecond ring reorientations with an energy barrier greater than 59 kilojoules per mole. This barrier is consistent with the temperature dependence of proton conductivity, suggesting that histidine-37 dynamically shuttles protons into the virion. We propose a proton conduction mechanism in which ring-flip–assisted imidazole deprotonation is the rate-limiting step.

Proton transport in synthetic materials is mediated either solely by hydrogen-bonded (H-bonded) water, as in hydrated ionic polymers (*1*), or solely by titratable heterocycles, such as imidazoles tethered to the backbone of anhydrous polymers (*2*). In comparison, the conduction mechanism of biological proton channels in cell membranes is more complex because both water and titratable protein sidechains are usually present (*3*). The influenza M2 protein forms a tetrameric proton channel that is important for the virus life cycle (*4*). Activated below pH 6, the M2 channel conducts 10 to 10,000 protons per second (*5*, *6*). The pH-sensing and proton-selective residue is a single histidine, His37, in the trans-

Department of Chemistry, Iowa State University, Ames, IA 50011, USA.

*To whom correspondence should be addressed. E-mail: mhong@iastate.edu

Science
AAAS

Fast Vesicle Fusion in Living Cells Requires at Least Three SNARE Complexes

Ralf Mohrmann, Heidi de Wit, Matthijs Verhage, Erwin Neher and Jakob B. Sørensen (September 16, 2010)
Science **330** (6003), 502-505. [doi: 10.1126/science.1193134]
originally published online September 16, 2010

Editor's Summary

Three's the Charm

The molecular machinery mediating membrane fusion during secretion from a cell requires a complex of so-called SNARE protein that forms a coiled bundle of four parallel α-helices. **Mohrmann *et al.*** (p. 502, published online 16 September) developed an elegant approach to find out how many SNARE complexes are required to promote secretion of individual secretory vesicles in living chromaffin cells by titrating the ratio of wild-type and mutant SNARE proteins expressed. For fast synchronous release, a minimum of three SNARE complexes per vesicle were required. Fewer SNARE complexes resulted in slower release.

Science (print ISSN 0036-8075; online ISSN 1095-9203) is published weekly, except the last week in December, by the American Association for the Advancement of Science, 1200 New York Avenue NW, Washington, DC 20005.

www.sciencemag.org/cgi/content/full/science.1193134/DC1

Supporting Online Material for

Fast Vesicle Fusion in Living Cells Requires at Least Three SNARE Complexes

Ralf Mohrmann,* Heidi de Wit, Matthijs Verhage, Erwin Neher, Jakob B. Sørensen*

*To whom correspondence should be addressed. E-mail: Ralf.Mohrmann@uks.de (R.M.); jakobbs@sund.ku.dk (J.B.S.)

Published 16 September 2010 on *Science* Express
DOI: 10.1126/science.1193134

This PDF file includes:

Supporting Online Material

Materials and methods

Chromaffin cell preparation and viral expression system. *Snap-25* null embryos were obtained by Cesarean section at E17-E18. Preparation of adrenal glands and cultivation of chromaffin cells were performed as described before (*S1*). Plasmids needed for generation of Semliki Forest viruses were generated by standard techniques of molecular biology. Starting from a cDNA encoding an N-terminal fusion construct between SNAP-25 and EGFP (*S2*) (here denoted EGFP-SN25B), we generated GFP-SN25B variants with either single (M71A or I192A) or double alanine substitutions in layer +5 by PCR mutagenesis. The generated PCR-fragments were cloned into a modified pSFV1 plasmid containing a multiple cloning site with unique Nsi I and BssH II restriction sites (courtesy of Ralf B. Nehring). To obtain mCherry-tagged versions of these SNAP-25 variants, appropriate PCR fragments of mCherry (*S3*) (mCh; kind gift of Dr. Roger Tsien) and mutated SN25B were generated, fused by PCR, and cloned into pSFV1 plasmid. Bicistronic expression units were constructed by fusing PCR-fragments of the polio virus-IRES sequence or the CITE-IRES sequence to PCR-fragments containing EGFP-SN25B or mCherry-SN25B M71A, I192A. The polio virus IRES sequence was adapted from an existing SFV transfer vector previously generated in our lab (*S4*). The EMCV IRES sequence was taken from pCITE2a (Novagen/Merck, Nottingham, UK) and further modified according to (*S5*) to yield attenuated versions. In an initial step of the cloning strategy we generated a fused PCR product containing the appropriate IRES sequence and the second open-reading frame either containing EGFP-SN25B or mCh-SN25BL5**. Care was taken to place the start-codon of the sequence at the right position with respect to the end of the IRES sequence. Due to a lack of restriction sites the generated PCR product was then fused to a fragment covering the downstream sequence of pSFV1 up to the

unique Spe I site. The resulting PCR product was finally inserted back into pSFV1 using the restriction sites BssH II and Spe I. In a second step an additional PCR fragment containing the sequence of the appropriate first open reading frame was generated and cloned into the modified pSFV1 vector using the restriction sites Nsi I and BssH II. All constructs were thoroughly sequenced before production of SFV particles. For experiments stored virus aliquots were activated by chymotrypsin cleavage, chymotrypsin was inactivated with aprotinin, and chromaffin cells were infected at days 2–4 after isolation. Electrophysiological recordings were performed at room temperature 5-8 h after infection with viruses.

Expression assays by Western blot and fluorescence intensity. The expression of tagged SNAP-25 variants after infection with bicistronic Semliki Forest viruses (SFV) was analyzed by Western blot and fluorescence intensity measurements. Cultured bovine chromaffin cells were prepared, infected, and subjected to Western blot analysis as described before (*S6*). Protein lysates were prepared under non-reducing conditions to allow for the formation of disulfide bonds, which results in characteristic band-shifts for GFP-tagged and mCherry-tagged SNAP-25 protein. Protein samples (30µg) were separated on 4-20% polyacrylamide-gels (Ready Gel; Bio-Rad Laboratories, Hercules, CA) and transferred onto nitrocellulose membranes (Amersham Hybond-ECL; GE Healthcare Bio-Sciences, Uppsala, Sweden). After protein transfer, the blot was cut at ~70kDA, and SNAP-25 variants were assayed with polyclonal anti-SNAP-25 (1:3,000, Synaptic Systems, Göttingen, Germany) on the lower molecular weight section of the blot. On the other part of the blot valosin–containing protein (VCP) served as loading control and was detected by monoclonal anti-VCP (1:3,000, Abcam, Cambridge, United Kingdom). Protein bands were visualized by chemoluminescence using an ECL detection kit

(SuperSignal, West Pico; Pierce Chemical, Rockford, IL). Quantification was done by densitometry using ImageJ software (National Institutes of Health, Bethesda, Maryland). The relative expression levels of both SNAP-25 variants were calculated from the band intensities of the characteristic, oxidized protein species. Note that the ratio of oxidized to reduced protein for both, GFP-SNAP-25 and mCh-SNAP-25, was constant under the used experimental conditions, and was determined in separate experiments. To obtain an estimate of the fraction [mCh-SNAP-25]/([mCh-SNAP-25]+[GFP-SNAP-25]) by fluorescence intensity measurements, we took microphotographs of infected bovine chromaffin cells just before preparing lysates for western blot analysis. Using appropriate filtersets we obtained pictures of GFP- and mCherry fluorescence at a fixed exposure time (8s). The intensities of GFP and mCherry fluorescence were quantified in randomly selected chromaffin cells (150-450 cells). A GFP-mCherry fusion protein was used as reference for the calculation of the relative expression of mCherry-tagged and GFP-tagged SNAP-25, as the fusion protein presents both fluorophors at a fixed ratio of 1:1.

Electrophysiology, electrochemistry, and calcium imaging. Flash photolysis of caged calcium, ratiometric measurements of intracellular calcium concentration, patch-clamp capacitance measurements, and amperometric recordings were performed as previously described (*S1, S7*). Secretion was elicited by flash photorelease of caged calcium and monitored in parallel by capacitance measurements and amperometric recordings, which ensured that mainly catecholamine release from dense-core vesicles was studied. To eliminate photo-artifacts from amperometric traces originating from the UV flash light, isolated artifacts were recorded after removal of the chromaffin cell using the patch pipette and subsequently subtracted from associated traces. Nitrophenyl-EGTA (NPE) used in calcium-uncaging experiments was obtained from Synaptic Systems (Göttingen, Germany).

Intracellular calcium concentrations were determined with two dyes (fura-4F and furaptra, Invitrogen) as described in earlier studies (Voets, 2000; Sørensen et al., 2002). Unlike previous studies, Vitamin C was added to the intracellular solution to minimize flash-induced damage to fura dyes. Fura-dyes were excited at 340nm and 370nm for ratiometric calcium determination. The composition of the intracellular solution was (in mM): 100 Cs-gluconate, 8 NaCl, 4 $CaCl_2$, 32 HEPES, 2 Mg-ATP, 0.3 GTP, 5 NPE, 0.4 fura-4F, 0.4 furaptra, and 1 Vitamin C, pH 7.2 (osmolarity was adjusted to 290 mOsm). The extracellular solution was (in mM): 145 NaCl, 2.8 KCl, 2 $CaCl_2$, 1 $MgCl_2$, 10 HEPES, pH 7.2 (osmolarity was adjusted to 300 mOsm). Data were analyzed using Igor Pro 6 software (Wavemetrics, Lake Oswego, OR). Analysis of release kinetic was performed by fitting capacitance traces with the sum of three exponential functions. As described earlier (*S1*), this approach allowed the distinction of the two burst components (denoted as 'fast burst' and 'slow burst' in the figures) and the quantification of their corresponding amplitudes and time constants (referred to as amplitudes A_{fast} and A_{slow} and time constants τ_{fast} and τ_{slow}). The third exponential is used for fitting the sustained component. If the fit identified a negative amplitude of at least one component, or if two time constants were closer than a factor two apart, fitting with a two exponential function (one exponential for the burst, one for the sustained component) was used instead. Time constants faster (smaller) than 50 ms were interpreted to describe release from the readily-releasable pool, while time constants between 50 and 500 ms were considered to represent fusion of vesicles from the slowly-releasable pool. It should be noted that some of our results indicate significant changes of both burst time constants, which indicates that both release processes are changed. In this case, a clean distinction of the two burst components (fast and slow) is not always possible. Results are generally given as mean±SEM in figures. If not marked otherwise, student's t-test (unpaired) was used for statistical comparisons.

Quantification of expression levels by intensity measurements in single cells. The relative expression ratios of mCh-SN25BL5** and EGFP-SN25B were determined by wide-field fluorescence intensity measurements within individual chromaffin cells right before electrophysiological recordings. Fluorophors were excited at appropriate wavelengths (mCh: 545 nm; EGFP: 475 nm) using a monochromator as lightsource (Polychrome II; Till Photonics, Gräfelfing, Germany). Fluorescence pictures were taken with an Imago CCD camera (Till Photonics) using matching dichroic mirrors (EGFP: HC Beamsplitter BS495; mCh: Q570LP) and emission filters (EGFP: HQ525/50m; mCh: HQ610/75M; all supplied by AHF Analysentechnik, Tübingen, Germany). Additional excitation filters (EGFP: HQ470/40; mCh: 545/30; AHF Analysentechnik, Tübingen) were used to suppress background white light emitted by the monochromator. Using this optical setup crosstalk between channels was estimated to be 1.5±0.5% for EGFP fluorescence in the mCherry channel and 0.6±0.2% for mCherry fluorescence in the GFP channel. Pictures were analyzed with TillVision 4.0 software (Till Photonics, Gräfelfing, Germany). Since viral expression caused accumulation of SNAP-25 protein within intracellular compartments, we restricted our analysis to regions extending 1-2 µm from the plasmamembrane. A virally expressed EGFP-mCherry fusion protein was employed to define a reference point with equimolar fluorophor ratio under our experimental conditions. Using this reference we calculated the fraction [mCh-SN25BL5**]/([mCh-SN25BL5**] +[EGFP-SN25B]) for each cell.

Colocalization of protein variants by confocal microscopy. Distribution patterns of mCh-SN25BL5** and EGFP-SN25B in chromaffin cells were studied using a confocal laser scanning microscope (LSM 710, Carl Zeiss Microimaging GmbH, Germany). Cultured mouse chromaffin cells were infected with bicistronic SFV mCh-SN25BL5** IRES EGFP-SN25B and imaged 5-6 h post

infection. Confocal sections of 0.8-0.9 µm (pinhole 1 Airy unit) were taken slightly above the foot area of each cells. EGFP and mCherry were excited at 488 nm and 543 nm, respectively. Images of EGFP and mCherry fluorescence were acquired sequentially with alternating laser excitation and separate channels using recommended detector presets for EGFP and mCherry (ZEN 2008 software, Carl Zeiss Microimaging GmbH). Detector gains of both channels were individually adjusted to cover the whole intensity range. Eight frames were taken in each channel in an alternating fashion and averaged to yield the final image. Only cells with moderate expression of both SNAP-25 variants were selected for analysis, as overly high expression levels lead to an almost homogenous protein distribution in cells. Image analysis was performed with ImageJ software. Using the popular "Just Another Colocalisation Plugin" (JACoP; (*S8*)) we analyzed the extent of colocalization between mCh-SN25BL5** and EGFP-SN25B. As reference we used the EGFP-mCh fusion protein, which by definition is expected to produce highly colocalized fluorescence signals. Crosstalk between channels under these experimental conditions was tested by imaging cells solely expressing EGFP or mCh-tagged SNAP-25. Using fixed gain settings for both detector channels we found 4.1±0.9% (n=18) crosstalk for EGFP in the mCh-channel and 1.1±0.2% (n=18) crosstalk for mCh in the EGFP-channel, respectively. Note that crosstalk of EGFP in the mCh-channel was likely overestimated in this control experiment due to the gain settings that favored the red channel over the green as well as due to the occurrence of background fluorescence.

Amperometric spikes. Amperometric spikes were recorded as previously described (*S1*). While amperometric recordings were performed with carbon fibers of 10 µm (Amoco Corp., Greenville, SC) during flash-photolysis experiments, we employed fibers of 5 µm diameter for recordings of single spikes in order to reduce noise. Due to a rapid ageing of the amperometric electrodes, we used freshly

prepared fibers for no more than two consecutive recordings. Fibers were clamped to +720mV, and amperometric current signals were amplified and prefiltered at 3 kHz using an EPC-7 (HEKA Elektronik, Lambrecht/Pfalz, Germany). For further analysis current traces were digitally filtered at 600 Hz (Gaussian filter) in Igor Pro. Amperometric spikes were detected (threshold 5pA) and analyzed with regard to amplitude, rise-time, halfwidth, and pre-spike foot duration/charge using a custom macro running in Igor Pro. To account for the significant cell-to-cell variability of amperometric data, and the fact that parameters are often not normally distributed, we relied on the cell median instead of the mean for our analysis. The medians of the waveform parameters were determined for each individual cell based on all recorded spikes, and the calculated medians were subsequently averaged within the experimental group and statistically compared. To ensure a sound estimation of the median only recordings with at least ten spikes were included in the analysis.

Electron microscopy of cultured chromaffin cells. Chromaffin cells from *Snap-25 -/-* (E18) mice were plated on rat tail type 1 collagen-coated coverslips (Cellocate, Eppendorf, Germany) and infected (DIV2, 2 days *in vitro*) with SFVs expressing either SN25B wild type or SN25B mutants harboring single (M71A or I192A) or double (M71A, I192A) mutations in layer +5. Cells were fixed for 45 min at room temperature with 2.5% glutaraldehyde in 0.1 M cacodylate buffer (pH 7.4), washed, embedded and analyzed as before (*S9-S11*). Analysis of secretory vesicle distribution was done blinded for the experimental condition. Docked vesicles were without any measurable distance between granule and plasma membrane.

Supporting text

The rosette model of SNARE-complexes

We wish to arrive at a mathematical expression for the expected secretion when two different SNARE species are incorporated into a rosette-like fusion complex driving secretion, and to establish a way to determine *n*, the number of SNARE-complexes in a rosette.

Assume we have two forms of SNAP-25, one at concentration $[S_1]$, which is functional, another one at concentration $[S_o]$, which is mutated and let x be the mole fraction of the mutant ($x = [S_o]/([S_1]+[S_o])$). We further assume that S_0 and S_1 forms compete for forming individual SNARE-complexes, and that they have affinity K towards some acceptor complex A.

$$A + S_0 \rightleftarrows AS_0 \qquad [AS_0] = K[A][S_0]$$

$$A + S_1 \rightleftarrows AS_1 \qquad [AS_1] = K[A][S_1]$$

We assume that a functional release apparatus is made up of *n* SNARE-complexes, possibly arranged in a rosette-like manner, and that AS_0 and AS_1 participate in such rosettes in proportion to their abundance. Then, the probability P_0 and P_1 that a given slot is filled with wildtype and mutant forms of SNARE-complexes, respectively, can be calculated according to

$$\frac{P_o}{P_1} = \frac{[S_o]}{[S_1]}; \qquad P_o + P_1 = 1;$$

yielding

$$P_1 = \frac{[S_1]}{[S_o]+[S_1]}; \quad P_o = \frac{[S_o]}{[S_o]+[S_1]} = x$$

Thus, P_0 is equal to the mole fraction of the mutant. The probability P_n that all of the *n* SNARE complexes in the rosette are occupied by S_1 (or else, that the complex is fully functional and displays wildtype kinetics):

(1) $$P_n = (P_1)^n = \left(\frac{[S_1]}{[S_o]+[S_1]} \right)^n = (1-x)^n$$

If the amplitude of the response Y (or else the amplitude of the component with wildtype kinetics) is assumed to be proportional to P_n, then

$$\text{Log Y} = \text{constant} + \text{n log } (1-x)$$

In this case, the slope of a plot of log *Y* versus *x* is:

(2) $$\frac{d \log Y}{dx} = -\frac{n}{1-x}$$

which for $x \ll 1$ reduces to $-n$.

For differential affinities of species S_o and S_1 towards the acceptor complex A, with α representing the ratio of affinity constants, a similar derivation yields $-n\alpha$ for the limiting slope in such a plot.

Thus the stoichiometry of the rosette (*n*) can be found by plotting the logarithm of the response size against *x*, the mol fraction of the mutation. The slope of the plot at low x-values will be $-n$ scaled by the relative affinities of the two SNARE species towards the assumed receptor *A*. In case the mutant SNARE-form (with concentration S_o) is not an absolute dominant-negative, such that secretion is still possible when one or more mutants are incorporated into the rosette, estimation of *n* is still possible using the same expressions, if the amplitude of unperturbed secretion can be identified and used in the place of *Y* (for instance if incorporation of one mutant molecule results in a detectable kinetic change of secretion).

Supporting Figures

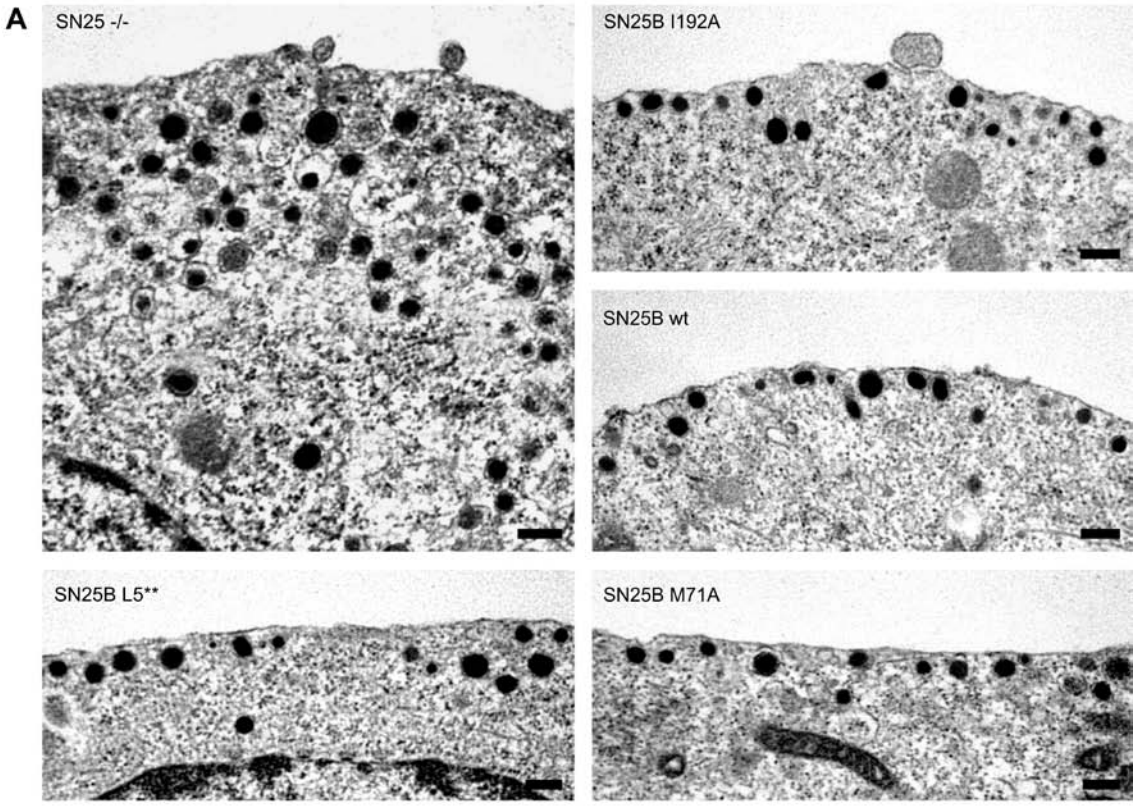

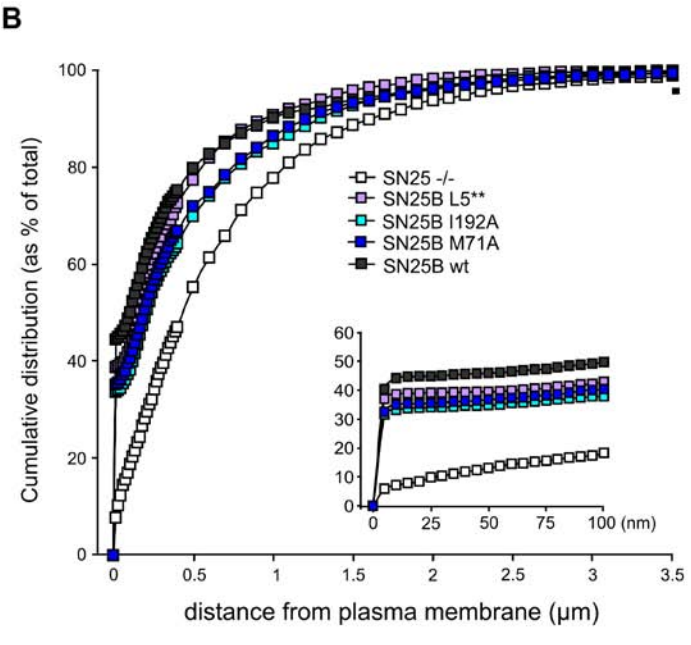

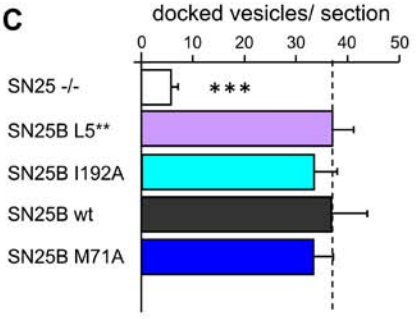

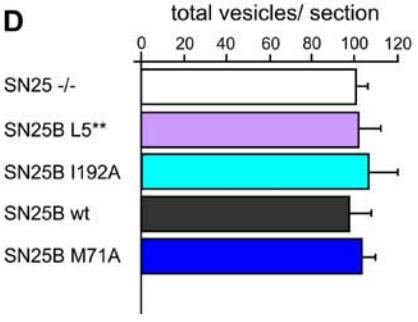

Fig. S1. Mutations interfering with Layer +5 do not compromise vesicle docking. *(A)* Electron micrographs from cultured *Snap-25* deficient chromaffin cells either untransfected (SN25 -/-) or expressing either wildtype SN25B or SN25B mutants harboring single or double mutations in layer +5. All constructs were N-terminally fused to EGFP with the exception of SN25BL5**, which was tagged with mCherry. Scalebars: 200 nm. *(B)* Normalized cumulative distribution of vesicles as a function of distance from the plasma membrane. Inset shows cumulative vesicle distribution in the sub-membrane region within 0–100 nm. *(C)* Number of docked vesicles per section (mean±SEM). *(D)* Total number of vesicles per section. For each condition 20 cells (n) and 5 animals (N) were analyzed in a blind fashion; data are means±SEM.

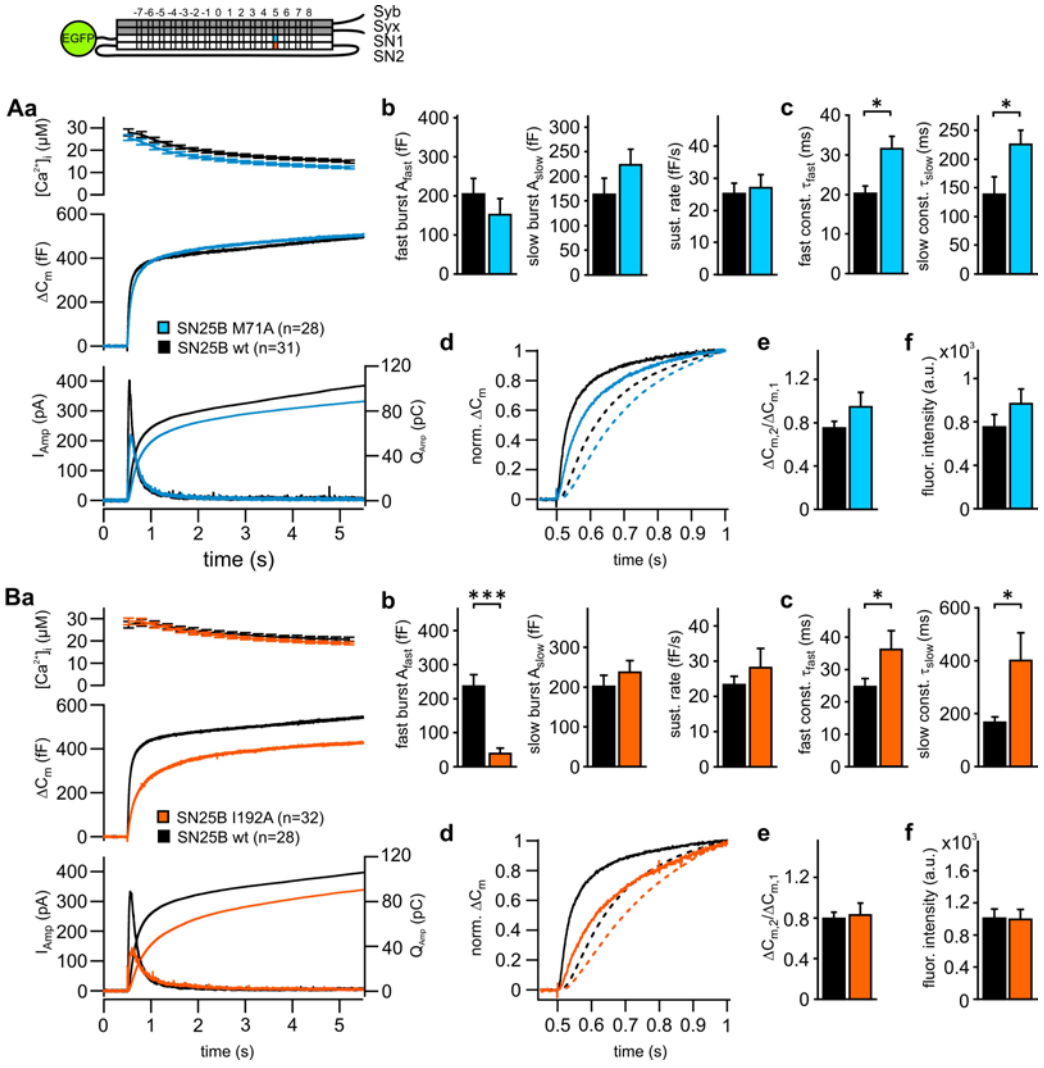

Fig. S2. Single alanine substitutions in layer +5 slow down dense-core vesicle release, but cause little inhibition of overall secretion. *Top panel:* Illustration of the position of both single amino acid exchanges. M71A is marked in blue; I192A is labeled in orange *(Aa)* Averaged data for *Snap-25* deficient chromaffin cells expressing wildtype EGFP-SN25B (SN25B wt, black, n = 31 cells) or GFP-SN25B-M71A (SN25BM71A, blue, n = 28). *Upper panel:* intracellular calcium concentration (mean ± SEM). *Middle panel:* averaged capacitance change obtained after calcium-uncaging. *Lower panel:* averaged amperometric current (thick lines, left axis) and cumulative amperometric charge (thin line, right axis). *(Ab, Ac)* The kinetic analysis of capacitance changes in SN25BM71A expressing cells

demonstrated significantly ($p<0.05$) increased fast and slow time constants, but no significant changes of the fast and slow burst amplitudes or the sustained release rate. The data are given as mean±SEM *(Ad)* Averaged capacitance change (solid lines) and cumulative amperometric charge (dashed lines) after normalization to highlight the slowdown of secretion mediated by SN25BM71A. *(Ae)* Recovery ($\Delta C_2/\Delta C_1$) of vesicle pools (mean±SEM) was assayed by applying a second flash 100 s later. *(Af)* Protein expression (mean±SEM) of both SNAP-25 variants as estimated by the intensity of their EGFP-tags. *(B)* Analysis of secretion in SNAP-25 deficient cells expressing SN25BI192A (SN25B I192A, orange, n = 32) compared to wildtype EGFP-SN25B (SN25B wt, black, n = 28). For an explanation of panels, see legend to A. *(Ba)* Mean secretion was reduced, and release was slowed down. *(Bb, Bc)* Fast and slow time constants (mean±SEM) were significantly ($p<0.05$) prolonged, and the amplitude of the fast burst (mean±SEM)was strongly depressed ($p<0.0001$). Sustained release was unchanged. *(Be)* Recovery and *(Bf)* protein expression (mean±SEM) were comparable to controls.

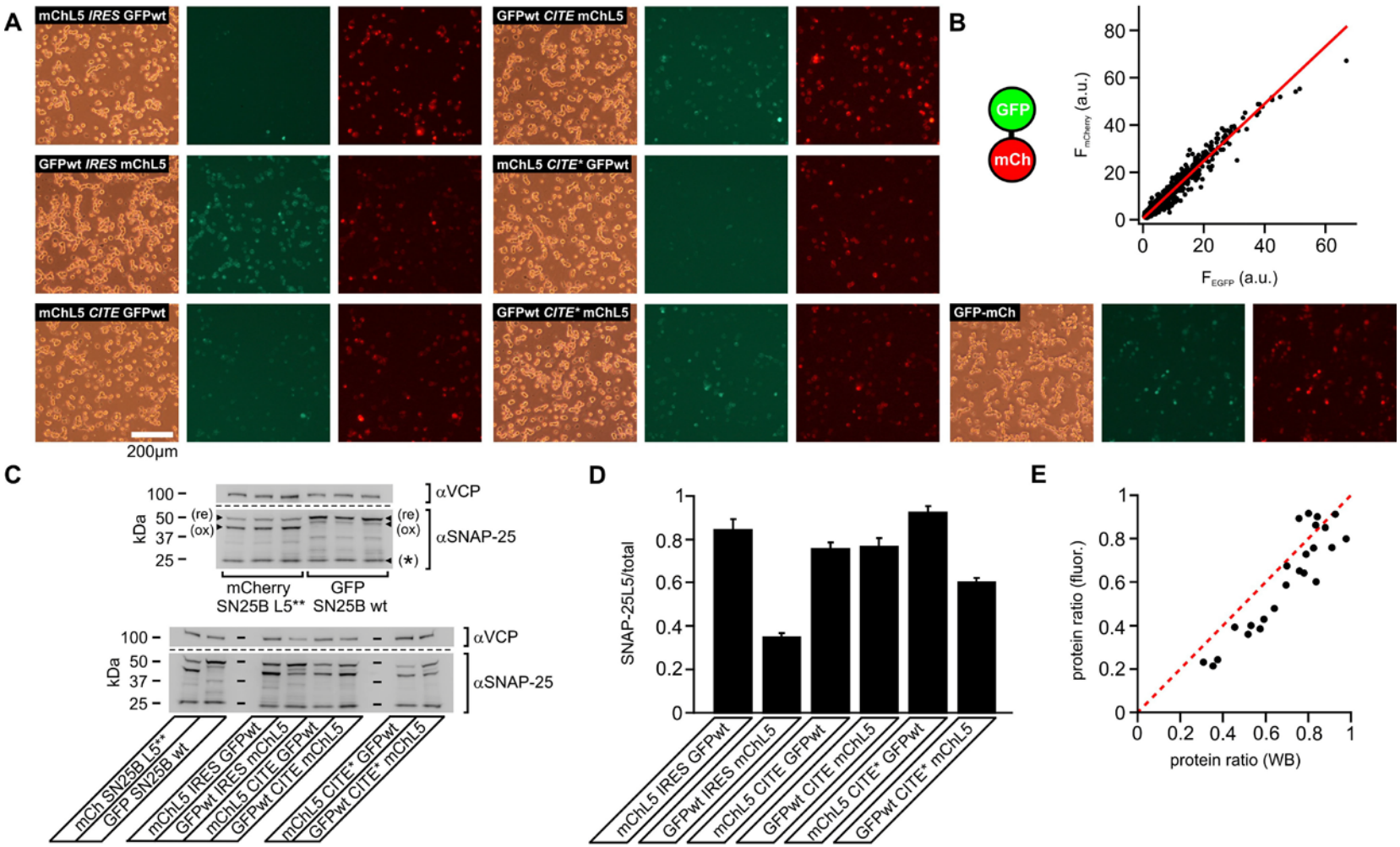
A
mChL5 IRES GFPwt
GFPwt CITE mChL5
GFPwt IRES mChL5
mChL5 CITE* GFPwt
mChL5 CITE GFPwt
GFPwt CITE* mChL5
GFP-mCh
200µm
B
GFP
mCh
F_mCherry (a.u.)
F_EGFP (a.u.)
C
kDa
100
50
37
25
(re)
(ox)
(*)
αVCP
αSNAP-25
mCherry SN25B L5**
GFP SN25B wt
mCh SN25B L5**
GFP SN25B wt
mChL5 IRES GFPwt
GFPwt IRES mChL5
mChL5 CITE GFPwt
GFPwt CITE mChL5
mChL5 CITE* GFPwt
GFPwt CITE* mChL5
D
SNAP-25L5/total
E
protein ratio (fluor.)
protein ratio (WB)

Fig. S3 Characterization of bicistronic Semliki Forest viruses. *(A)* Microphotographs of cultured bovine chromaffin cells infected with bicistronic Semliki Forest (SF) viruses expressing both mCherry-SN25BL5** (mChL5) and wildtype EGFP-SN25B (GFPwt). Each panel contains a transmission (*left*), EGFP fluorescence (*middle*), and mCherry fluorescence (*right*) image. The corresponding virus type is indicated on top of each panel. *(B)* Virally expressed EGFP-mCherry fusion protein was used as a reference for calculation of the fraction of mCh-SN25BL5** expression. *Lower panel*: Transmission image (*left*), EGFP fluorescence (*middle*), mCherry fluorescence (*right*). *Upper panel:* A plot of the EGFP- versus mCherry fluorescence intensity demonstrates a constant intensity ratio for equimolar amounts of EGFP and mCherry fluorophors (*upper panel*), which was used to determine a constant for transforming intensity ratios into protein ratios. (*C*) Western blot analysis of bovine chromaffin cells following infection by viruses. mCherry-tagged and EGFP-tagged SNAP-25 exhibits differential formation of oxidized species under non-reducing Western blot conditions (*upper panel*). Reduced SNAP-25 variants are marked "re"; oxidized species are labeled as "ox". Untagged, endogenous protein is indicated by "*". Note the constant ratio of oxidized and reduced species within three independent samples for mCh-SN25BL5** and EGFP-SN25B. The lower panel depicts a blot of lysates obtained from bovine chromaffin cells infected with six different dicistronic SF viruses. Valosin–containing protein (VCP) was used as loading control in all Western Blot experiments. *(D)* Quantification of Western blot data (three sets of independent samples), given as mean±SEM. *(E)* Comparison of Western blot data and fluorescence intensity measurements. Each data point in the plot represents analysis results derived from the same sample of cultured bovine chromaffin cells. An ideal correlation of data from both analyses methods would place data points on the dashed identity line.

Given the semi-quantitative nature of Western blot data, results obtained by both methods are well matched.

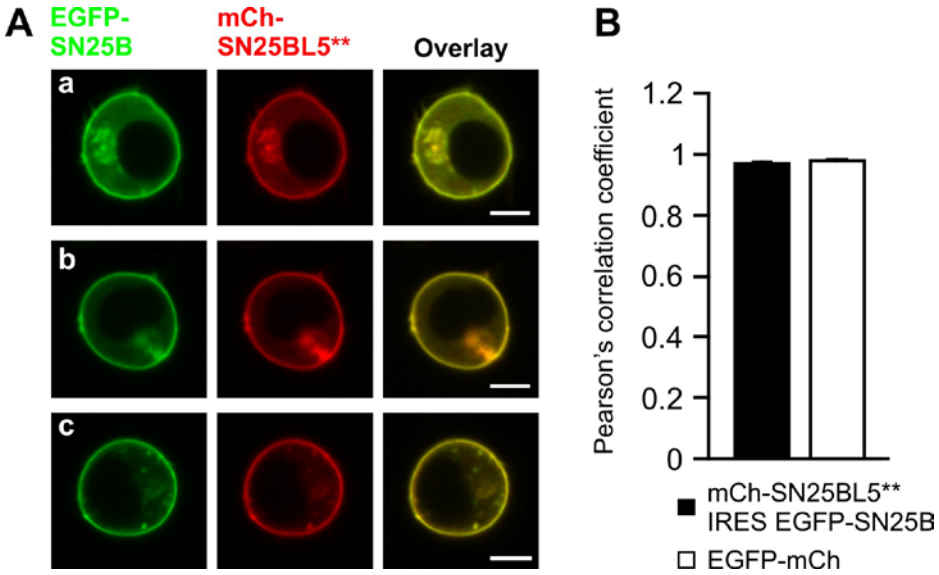

Fig. S4 Cellular distribution of mutant SNAP-25 is indistinguishable from wildtype protein. *(A)* Example microphotographs of cultured mouse chromaffin cells co-expressing mCh-SN25BL5** and EGFP-SN25B (a-c). In each panel left images depict EGFP fluorescence (green), middle images show mCh fluorescence (red), and right pictures present the overlay of both signals. Note that intracellular aggregation of virally expressed protein can vary between cells. The expression pattern of mCh-SN25BL5** overlapped with EGFP-SN25B. *(B)* Colocalisation was quantified based on Pearson's correlation coefficient. For mCh-SN25BL5** and EGFP-SN25B Pearson's coefficient was near 1 (0.970±0.004; n=46) indicating strong colocalisation of both proteins. EGFP-mCh fusion protein was used as reference and yielded a comparably high Pearson's coefficient (0.978±0.005; n=17). Data are given as mean±SEM.

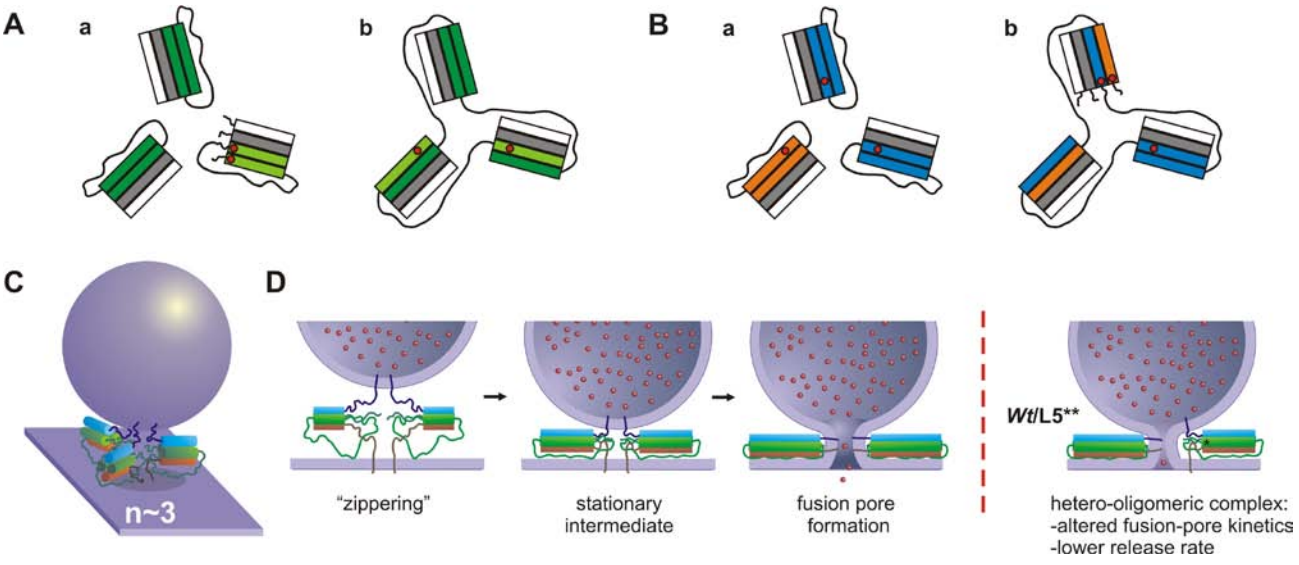

Fig. S5 Schemes of fusion. *(A)* Incorporation of SN25BL5** in rosettes together with wildtype protein separates the single mutations (red dots) if domain-swapping occurs (b), whereas in the absence of domain-swapping (a), the two single mutations always join the same SNARE-complex. *(B)* Test of domain-swapping hypothesis: coexpression of the two single mutations (M71A and I192A) in the presence of domain-swapping (b) regenerates the catastrophic SN25BL5** mutation in some SNARE-complexes, whereas if domain-swapping does not occur, the single mutations always stay separate (a). The experiments presented in Fig. 4 in the main manuscript argue against domain-swapping. *(C)* Cartoon showing three SNARE-complexes mediating fast vesicle fusion. *(D)* The 'zippering' of the SNARE complexes pulls both membranes together and is followed by fusion pore formation and full fusion. Right panel: SN25BL5** probably reaches the intermediate state normally, but possesses a defect in the assembly of the C-terminal end of the complex and therefore cannot contribute to final fusion. Heteromeric rosettes are characterized by lower fusion rates and altered amperometric spike waveform.

Supporting references

S1. J. B. Sorensen *et al.*, *Cell* **114**, 75 (Jul 11, 2003).

S2. I. Delgado-Martinez, R. B. Nehring, J. B. Sorensen, *J Neurosci* **27**, 9380 (Aug 29, 2007).

S3. N. C. Shaner *et al.*, *Nat Biotechnol* **22**, 1567 (Dec, 2004).

S4. J. B. Sorensen *et al.*, *Proc Natl Acad Sci U S A* **99**, 1627 (Feb 5, 2002).

S5. Y. A. Bochkov, A. C. Palmenberg, *Biotechniques* **41**, 283 (Sep, 2006).

S6. G. Nagy *et al.*, *J Neurosci* **22**, 9278 (Nov 1, 2002).

S7. J. B. Sorensen *et al.*, *Embo J* **25**, 955 (Mar 8, 2006).

S8. S. Bolte, F. P. Cordelieres, *J Microsc* **224**, 213 (Dec, 2006).

S9. R. F. Toonen *et al.*, *EMBO J.* **25**, 3725 (Aug 23, 2006).

S10. H. de Wit *et al.*, *Cell* **138**, 935 (Sep 4, 2009).

S11. H. de Wit, L. N. Cornelisse, R. F. Toonen, M. Verhage, *PLoS ONE* **1**, e126 (2006).